Handover Probability Analysis in Multi-Tier Aerial Networks at Varying Altitudes

Fahd Ahmed Khan[1], Haneya Naeem Qureshi[1], Ali Imran[1,2] and Hazem Refai[1].
[1]AI4Networks Research Center, School of Electrical & Computer Engineering, University of Oklahoma, OK, USA.
[2]James Watt School of Engineering, University of Glasgow, United Kingdom.
Email: {fahd.khan,haneya,ali.imran,hazem}@ou.edu.

***Abstract*—Existing works on user mobility in unmanned aerial vehicle (UAV)/drone-based aerial networks consider either fixed height drone base stations (DBSs), or are limited to two-tier networks only, and do not take into account tier association biasing, which is important for developing intelligent traffic offloading and load balancing schemes to support the diverse use cases enabled by emerging networks. This paper addresses these gaps by analyzing the impact of user mobility in a multi-tier UAV heterogeneous network at varying heights serving ground users and taking into account the biased average receive power association, where each tier has an independent cell range extension (CRE) factor. We evaluate the handover probability of a mobile user by first deriving the distance distributions to the serving DBS and the probability of user association with a DBS of a specific tier. The quantification and insights from our theoretical analysis, corroborated with numerical simulations reveal that the probability of handover (dependent on the CRE factor of the tiers, height of the DBSs and velocity) must be optimized in tandem with coverage probability for optimal network performance.**

***Index Terms*—UAV/drone based aerial networks, emerging cellular networks, mobility, handover probability, multi-tier networks, cell range extension.**

I. Introduction

Unmanned aerial vehicles (UAVs) are envisioned to be part of emerging wireless cellular networks because of their capability to enable rapid on–demand services and expand coverage and capacity at a low cost by acting as aerial/drone base stations (DBS) [1], [2]. They can thus serve in emergency scenarios such as natural disasters when a ground base station (BS) malfunctions, or complement existing BSs for short-term social gatherings when they are overloaded with user equipments (UEs) to provide service in that region [1].

In order to support the heterogeneous requirements of a diverse range of future applications such as high data-rate extended reality, ultra-reliable low latency communication for autonomous vehicles and energy efficient communication for energy constrained surveillance systems [3], both cellular and aerial networks are envisioned to have a dense multi-tier heterogeneous network architecture [1], [3], [4]. The terrestrial BSs and aerial DBSs will be densely deployed to improve the area spectral efficiency (ASE) of the network. Dense deployment of BSs brings the UE closer to them, thus reducing the pathloss and improving the received signal power. In addition, it enables reuse of the limited frequency spectrum to enhance network capacity [3]. A drawback of dense deployment is that the cell size reduces resulting in frequent handovers. Continuous connectivity becomes challenging, and these frequent handovers lead to a decline of user experience and heavy signaling overheads [5].

Therefore, for such dense cellular networks, accurate mobility modeling of the network is essential for the optimization of key mobility-related performance indicators (KPIs) such as handoff rate, handoff probability, ping-pong events and sojourn time, that are crucial for UE quality of experience [5]. Two approaches have been adopted to analyze the aforementioned KPIs, namely, 1) trajectory based analysis; evaluates the number of intersections between the user trajectory and the cell boundaries and 2) measurement based analysis; based on received signal power at the UE [6], [7].

In [8], the measurement based approach was adopted and the handover probability was analyzed for a multi-tier 3D UAV network where each tier had a different altitude. In [9], authors adopted the same approach to analyze the handover probability when the DBSs are hovering in random directions at a constant height. They analyzed the scenarios of DBSs moving with the same speed and different speeds and showed that the same speed scenario is equivalent to the single-tier terrestrial cellular network, in which the BSs are static and UEs are mobile. The sojourn time and handover rate for a fixed height UAV network was analyzed in [10] and it was shown that the handover rate is minimum when DBSs move with the same speed.

The trajectory based approach was adopted in [11] to analyze the handover rate for mobile aerial UEs of varying altitudes served by a terrestrial network. It was shown that vertical movements have a low handover rate. In [12], handover rate for a two-tier terrestrial network with varying antenna height and biased association was studied. By replacing the antenna heights with DBS heights, one can obtain the handover rate for an aerial cellular network.

In these previous works, either the nearest distance association without tier association biasing was investigated [8]–[11], or the analysis was limited to that of a two-tier network only [12]. Consideration of association bias corresponding to each tier is important as we can flexibly control the load of each tier by tuning the cell range extension (CRE) factor, and thus develop intelligent traffic offloading and load balancing schemes needed to cater for the needs of emerging heterogeneous networks. It was shown in [13], that multi-tier terrestrial networks with biased averaged received power association lead to non-convex cell boundaries making the analysis non-trivial. Following a similar approach to [13], in this work, we present a general framework to analyze

This work is supported by the National Science Foundation under Grant Number 1923669 and NASA under Proposal# 20-2020EPSCoR-0014.

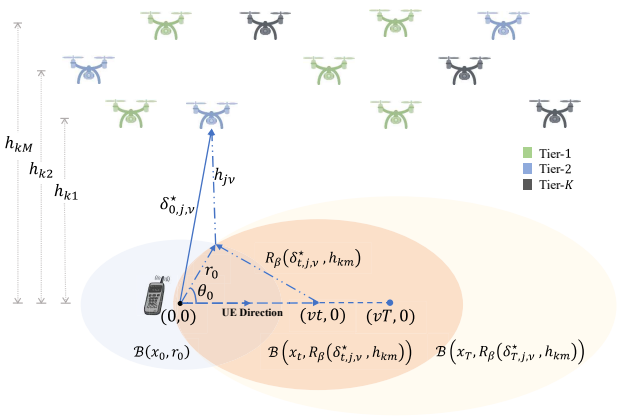

Fig. 1: System Model.

the handover probability of a multi-tier aerial network with varying altitudes, where UE association is based on the biased averaged received power. While authors in [13] adopted an approximation to derive the approximate handover probability, we utilize the theory of family of curves to obtain the exact expression of handover probability, which is an important KPI used to calculate the sojourn time and handoff rate [6], [10], [13]. These KPIs enable analysis of other important network parameters such as channel occupancy time and call dropping probability during handoff. For deriving the handover probability expression, we also derive the association probability and distance distribution expressions. The results and analysis, corroborated through numerical simulations, show that tier-biasing and altitude adjustment can lead to a lower handoff probability and therefore, they must be set appropriately.

II. System Model

We consider a K-tier aerial network where the spatial distribution of the DBSs of the k-th tier, $k \in \{1, 2, ..., K\}$, follows an independent homogeneous Poisson Point Process (PPP) Φ_k with intensity Λ_k. Each tier is assumed to consist of DBSs at different altitudes. Without a loss of generality, the mobile user (UE) is assumed to be at the ground level.

For modeling the altitudes, we propose that a DBS can hover at M possible heights. The set of heights for DBSs belonging to the k-th tier is given as $\mathcal{H}_k = \{h_{k1}, h_{k2}, ..., h_{kM}\}$, where h_{km} denotes the m-th height in tier-k. The density of DBSs of height m in tier-k is denoted by λ_{km}, respectively, where $\Lambda_k = \sum_{m=1}^{M} \lambda_{km}$. Note that this model is general and the values of heights and corresponding densities may be different for each tier. Increasing the value of M, this model can scale to large networks with DBSs at many different altitudes [1].

Association Criteria: Different from the existing works [8]–[12], the UE associates to the DBS which provides the maximum biased average receive power. The association criteria, at time t, can be expressed as

$$\mathbb{D}_t(j,\nu) = \arg \max_{\substack{y_k \in \Phi_k \\ \forall k,m}} P_k B_k \left(\|x_t - y_{km}\|^2 + h_{km}^2 \right)^{-\frac{\alpha}{2}}, \quad (1)$$

[1]This model and the analysis in this work is also valid for terrestrial networks where BSs have antennas at different heights.

where $\mathbb{D}_t(j,\nu)$ is the serving DBS at height $h_{j\nu}$ belonging to tier-j, x_t is location of the UE at time t, y_{km} denotes the DBS location of the k-th tier and height h_{km}, P_k is the DBS transmission power of tier-k, B_k is the cell range extension (CRE) bias factor for tier-k and α is the path-loss exponent. The biased averaged received power association rule in (1) within multi-tier DBSs leads to non-convex cell boundaries making the analysis non-trivial [13].

At time $t = 0$, a typical UE is assumed to be at the origin, i.e., $x_0 = (0, 0)$ and based on (1), the UE associates to a DBS of tier-j at height $h_{j\nu}$, denoted by $\mathbb{D}_0(j,\nu)$.[2] Location of this serving DBS in the xy-plane is denoted by $\mathbf{y}_0$ which can be represented in polar form as $\mathbf{y}_0 = r_0 \angle \theta_0$. As shown in Fig. 1, the UE is assumed to move in a straight line along the positive x-axis with a constant velocity v for a duration T. UE movement in any direction can be modeled as this straight-line along the positive x-axis due to the stationarity and isotropicity of the homogeneous PPP [6], [13]. Position of the UE at any intermediate time t, is given as $x_t = (vt, 0)$ and its final location is denoted by $x_T = (vT, 0)$. At arbitrary time t, the UE to serving DBS radial distance (distance along the xy-plane) is $r_t = \|x_t - \mathbf{y}_0\| = \|x_t - r_0 \angle \theta_0\| = r_0^2 + v^2 t^2 - 2 r_0 v t \cos(\theta_0)$. The UE to serving DBS distance in 3D is obtained as $\delta^{\star}_{t,j,\nu} = \sqrt{r_t^2 + h_{j\nu}^2}$.

III. Probability of Tier Association & Distance Distributions

Proposition 1. *The probability density function (PDF) of distance between UE and the nearest DBS of tier-k and height m at time t, denoted as $\delta_{t,k,m} = \sqrt{r_t^2 + h_{km}^2}$, is given as*

$$f_{\delta_{t,k,m}}(z) = 2\pi\lambda_{km} z e^{-\pi\lambda_{km}\left(z^2 - h_{km}^2\right)} u\left(z^2 - h_{km}^2\right), \quad (2)$$

where $u(\cdot)$ denotes the unit step function.

Proof: The cumulative distribution function (CDF) of $\delta_{t,k,m}$ is given as $F_{\delta_{t,k,m}}(z) = \Pr\left(\sqrt{r_t^2 + h_{km}^2} < z\right)$ where r_t^2 is exponential random variable (RV) with mean $\frac{1}{\pi\lambda_{km}}$. As the distances are positive, the CDF can be written as $F_{\delta_{t,k,m}}(z) = \Pr\left(r_t^2 < z^2 - h_{km}^2\right)$ which is evaluated to yield

$$F_{\delta_{t,k,m}}(z) = \begin{cases} 0 & z^2 \le h_{km}^2 \\ 1 - e^{-\pi\lambda_{km}\left(z^2 - h_{km}^2\right)} & z^2 > h_{km}^2 \end{cases} \quad (3)$$

Taking the derivative of (3) yields (2). ■

From (2), it can be noted that the distance $\delta_{t,k,m}$ will always be greater than the DBS height.

Proposition 2. *The minimum distance from the UE, at time t, to DBSs of all tiers and heights excluding the tier-j DBSs at height ν, is given by $\delta_{t,!j,!\nu} = \min_{\{k,m\}\setminus\{k=j\,\&\,m=\nu\}} \beta_{jk}\delta_{t,k,m}$. The CDF of $\delta_{t,!j,!\nu}$ is*

$$F_{\delta_{t,!j,!\nu}}(z) = 1 - e^{-\pi \sum_{\substack{\{k,m\}\setminus \\ \{k\neq j\&m\neq\nu\}}} \lambda_{km}\left(\beta_{kj}^2 z^2 - h_{km}^2\right) u\left(\beta_{kj}^2 z^2 - h_{km}^2\right)}, \quad (4)$$

[2]Without a loss of generality, the UE and DBS location is characterized only in the xy-plane and the height, taken along z-axis, is mentioned separately.

where $\sum_{\{k,m\}}$ *is shorthand notation for* $\sum_{k=1}^{K}\sum_{m=1}^{M}$ *and* $\beta_{kj}=\left(\frac{P_kB_k}{P_jB_j}\right)^{\frac{1}{\alpha}}=\beta_{jk}^{-1}$.

Proof: The CDF of $\delta_{t,!j,!\nu}$ is expressed as $F_{\delta_{t,!j,!\nu}}(z)=\Pr\left\{\min_{\{k,m\}\setminus\{k=j\,\&\,m=\nu\}}\beta_{jk}\delta_{t,k,m}<z\right\}=1-\Pr\left\{\min_{\{k,m\}\setminus\{k=j\,\&\,m=\nu\}}\beta_{jk}\delta_{t,k,m}>z\right\}$. As the distances are independent, the CDF can be written as

$$F_{\delta_{t,!j,!\nu}}(z)=1-\prod_{\{k,m\}\setminus\{k=j\,\&\,m=\nu\}}\left(1-F_{\delta_{t,k,m}}\left(\beta_{kj}z\right)\right), \tag{5}$$

where $\prod_{\{k,m\}}$ is shorthand for $\prod_{k=1}^{K}\prod_{m=1}^{M}$. Substituting the CDF from (3) into (5) and after some simplification yields (4). ∎

It can be noted that $\beta_{kj}\in(0,\infty)$. $\beta_{kj}>1$ implies a bias towards tier-k, whereas $\beta_{kj}<1$ implies a bias towards the serving tier-j. Using results from Propositions 1 and 2, we derive the probability of association with a DBS of height $h_{j\nu}$ in tier-j and the distribution of UE to serving DBS distance given that the UE is associated with a DBS at height $h_{j\nu}$ in tier-j. These results are given in the following Proposition 3 and 4, respectively.

Proposition 3. *Let* $\mathbb{A}_{j,\nu}^{\star}$ *denote the event that the typical UE is served by a tier-*j *DBS at height* $h_{j\nu}$*, then the probability of event* $\mathbb{A}_{j,\nu}^{\star}$ *is given as*

$$\Pr\left(\mathbb{A}_{j,\nu}^{\star}\right)=2\pi\lambda_{j\nu}\int_{z>h_{j\nu}}e^{-\pi\sum_{\{k,m\}}\lambda_{km}\left(\beta_{kj}^2z^2-h_{km}^2\right)u\left(\beta_{kj}^2z^2-h_{km}^2\right)}dz. \tag{6}$$

Proof: The UE is associated with a DBS at height $h_{j\nu}$ in tier-j if $\delta_{t,j,\nu}<\beta_{jk}\delta_{t,!j,!\nu}$. Therefore, probability of event $\mathbb{A}_{j,\nu}^{\star}$ is expressed as $\Pr\left(\mathbb{A}_{j,\nu}^{\star}\right)=\Pr\left(\delta_{t,j,\nu}<\beta_{jk}\delta_{t,!j,!\nu}\right)$. We can evaluate this probability using the CDF of $\delta_{t,!j,!\nu}$ and PDF of $\delta_{t,j,\nu}$ as

$$\Pr\left(\mathbb{A}_{j,\nu}^{\star}\right)=\int_0^{\infty}\left(1-F_{\delta_{t,!j,!\nu}}\left(\beta_{kj}z\right)\right)f_{\delta_{t,j,\nu}}\left(z\right)dz. \tag{7}$$

Substituting the PDF from (2) and CDF from (4) into (7) and performing some mathematical manipulations yields (6). ∎

(6) shows that as $h_{j\nu}$ increases, the lower limit of the integral increases and as a result the probability that typical UE is served by a tier-j DBS at height $h_{j\nu}$, $\Pr\left(\mathbb{A}_{j,\nu}^{\star}\right)$, reduces. Similarly, increasing β_{kj} increases the argument of the exponential function and as a result $\Pr\left(\mathbb{A}_{j,\nu}^{\star}\right)$ reduces.

Proposition 4. *The typical UE to serving DBS distance is denoted as* $\delta_{t,j,\nu}^{\star}=\sqrt{r_t^2+h_{j\nu}^2}$*. The CDF of* $\delta_{t,j,\nu}^{\star}$ *is given as*

$$F_{\delta_{t,j,\nu}^{\star}}\left(z|\mathbb{A}_{j,\nu}^{\star}\right)=1-\frac{2\pi\lambda_{j\nu}}{\Pr\left(\mathbb{A}_{j,\nu}^{\star}\right)}\int_{y>h_{j\nu}}^{\infty}ye^{-\pi\sum_{\{k,m\}}\lambda_{mk}\left(\beta_{kj}^2y^2-h_{mk}^2\right)u\left(\beta_{kj}^2y^2-h_{mk}^2\right)}dy. \tag{8}$$

The PDF is obtained by taking the derivative of CDF in (8) *yielding*

$$f_{\delta_{t,j,\nu}^{\star}}\left(z|\mathbb{A}_{j,\nu}^{\star}\right)=\frac{2\pi\lambda_{j\nu}z}{\Pr\left(\mathbb{A}_{j,\nu}^{\star}\right)}e^{-\pi\sum_{\{k,m\}}\lambda_{mk}\left(\beta_{kj}^2z^2-h_{mk}^2\right)u\left(\beta_{kj}^2z^2-h_{mk}^2\right)}u\left(z-h_{j\nu}\right). \tag{9}$$

Proof: CDF of $\delta_{t,j,\nu}^{\star}$ is defined as

$$F_{\delta_{t,j,\nu}^{\star}}\left(z|\mathbb{A}_{j,\nu}^{\star}\right)=1-\Pr\left(\delta_{t,j,\nu}>z|\delta_{t,j,\nu}<\beta_{jk}\delta_{t,!j,!\nu}\right). \tag{10}$$

Representing the conditional probability in terms of joint probability yields

$$F_{\delta_{t,j,\nu}^{\star}}\left(z|\mathbb{A}_{j,\nu}^{\star}\right)=1-\frac{\Pr\left(\delta_{t,j,\nu}>z\cap\delta_{t,j,\nu}<\beta_{jk}\delta_{t,!j,!\nu}\right)}{\Pr\left(\delta_{t,j,\nu}<\beta_{jk}\delta_{t,!j,!\nu}\right)}. \tag{11}$$

Representing the probability in terms of an integral yields

$$F_{\delta_{t,j,\nu}^{\star}}\left(z|\mathbb{A}_{j,\nu}^{\star}\right)=1-\frac{1}{\Pr\left(\mathbb{A}_{j,\nu}^{\star}\right)}\int_{y>z}^{\infty}\left(1-F_{\delta_{t,!j,!\nu}}\left(\beta_{kj}y\right)\right)f_{\delta_{t,j,\nu}}\left(y\right)dy. \tag{12}$$

Substituting the PDF from (2) and CDF from (4) into (12) and performing some mathematical manipulations yields (8). ∎

IV. Probability of Handover

We define the handoff event when the UE changes DBS association after moving closer to another DBS (belonging to the same tier or a different tier) having a better biased averaged received power. The probability of handover, $\Pr(\mathbb{H})$, can be calculated using probability of the complementary event that the handover does not occur [6]. Handover will not occur for time duration, $t\in[0,T]$, if the mobile UE remains connected to the same DBS for the whole duration.

Equivalently, it can be stated that a handover will not occur if there is no other DBS within a surrounding circular region of radius equal to the radial distance between UE and DBS. At $t=0$, the typical UE at origin associates with the DBS of height $h_{j\nu}$ at $r_0\angle\theta_0$. This association implies that there is no other DBS closer than it i.e. $\Phi_j\left(\mathcal{B}\left(x_0,r_0\right)\right)=0$, where $\Phi_j\left(A\right)$ denotes the number of points of the PPP Φ_j, in a region A and $\mathcal{B}\left(x,r\right)$ denotes a 2D ball in the xy-plane with radius r centered at x.

As the UE moves along the positive x-axis with velocity v for a duration t, again handover will not occur if there is no other DBS closer than the associated DBS i.e. for arbitrary t, the ball $\mathcal{B}\left((vt,0),r_t\right)$ should not contain any DBS. If this holds for all positions of the UE, i.e. the *void region* $\mathcal{A}=\cup_{t\in[0,T]}\mathcal{B}\left((vt,0),r_t\right)\setminus\mathcal{B}\left(x_0,r_0\right)$ has no other DBS, then there will be no handover. Here, $\cup_t$ denotes the union operator over time t and $S_1\setminus S_2$ represents the set of elements of S_1 which are not elements of S_2. Region $\mathcal{B}(x_0,r_0)$ has been excluded because initial association to a DBS at time $t=0$ inherently implies $\Phi_j\left(\mathcal{B}\left(x_0,r_0\right)\right)=0$.

Let $\mathbb{N}_{\mathbb{H}}$ represent the event that there is no handover, then probability of this event is given as $\Pr\left(\mathbb{N}_{\mathbb{H}}\right)=\Pr\left(\Phi_j\left(\mathcal{A}\right)=0\right)$. The probability of this no handover event can be calculated using void probability of a PPP as $\Pr\left(\mathbb{N}_{\mathbb{H}}\right)=\exp\left(-\Lambda_j\left|\mathcal{A}\right|\right)$, where $|A|$ denotes the area of region A and Λ_j denotes the intensity of the PPP Φ_j.

Given that at time t, the UE is at location $x_t=(vt,0)$ and is connected to a DBS of tier-j and height $h_{j\nu}$, handover to any k-th tier DBS of height h_{km}, will not occur if there is no such DBS within a region $\mathcal{B}\left(x_t,\sqrt{\beta_{kj}^2\left(r_t^2+h_{j\nu}^2\right)-h_{km}^2}\right)=$

$\mathcal{B}\left(x_t, \sqrt{\beta_{kj}^2 {\delta_{t,j,\nu}^\star}^2 - h_{km}^2}\right)$. Let $R_\beta\left(\delta_{t,j,\nu}^\star, h_{km}\right) = \sqrt{\beta_{kj}^2 {\delta_{t,j,\nu}^\star}^2 - h_{km}^2}$, then depending upon the height h_{km} of the neighboring DBS, following observations can be made for the case when $\beta_{kj} = 1$,

1) $R_1\left(\delta_{t,j,\nu}^\star, h_{km}\right)$ must be greater than 0 which requires that $h_{km}^2 < \delta_{t,j,\nu}^\star = r_t^2 + h_{j\nu}^2$, i.e. a DBS can be considered for handover only if its height $h_{km} < \delta_{t,j,\nu}^\star$, otherwise $\Pr\left(\mathbb{N}_\mathbb{H}\right) = 1$.
2) If $h_{j\nu} < h_{km} < \delta_{t,j,\nu}^\star$, then $R_1\left(\delta_{t,j,\nu}^\star, h_{km}\right) < r_t$, implying $\left|\mathcal{B}\left(x_t, R_1\left(\delta_{t,j,\nu}^\star, h_{km}\right)\right)\right| < \left|\mathcal{B}\left(x_t, r_t\right)\right|$, i.e. if the neighboring DBS height is higher, the void region where there should be no DBS of height h_{km}, shrinks.
3) If $h_{km} \leq h_{j\nu} < \delta_{t,j,\nu}^\star$, then $R_1\left(\delta_{t,j,\nu}^\star, h_{km}\right) \geq r_t$, implying $\left|\mathcal{B}\left(x_t, R_1\left(\delta_{t,j,\nu}^\star, h_{km}\right)\right)\right| \geq \left|\mathcal{B}\left(x_t, r_t\right)\right|$ i.e. if the neighboring DBS height is lower, the void region expands.

When the DBSs are at the same height i.e. $h_{j\nu} = h_{km}$, then $\mathcal{B}\left(x_0, R_1\left(\delta_{0,j,\nu}^\star, h_{km}\right)\right) = \mathcal{B}\left(x_0, r_0\right)$ and $\mathcal{B}\left(x_0, R_1\left(\delta_{T,j,\nu}^\star, h_{km}\right)\right) = \mathcal{B}\left(x_T, r_T\right)$. In this case, these regions will always intersect and area of the region can be calculated by the union of $\mathcal{B}\left(x_0, r_0\right)$ and $\mathcal{B}\left(x_T, r_T\right)$ [13]. However, this is not necessary when DBSs are at different heights i.e. $h_{j\nu} \neq h_{km}$ or when $\beta_{kj} \neq 1$. In this case, $\mathcal{B}\left(x_0, R_\beta\left(\delta_{0,j,\nu}^\star, h_{km}\right)\right)$ and $\mathcal{B}\left(x_T, R_\beta\left(\delta_{T,j,\nu}^\star, h_{km}\right)\right)$ expand or contract and thus, may not intersect. So for calculation of $\Pr\left(\mathbb{N}_\mathbb{H}\right)$, similar to [13], we have different cases.

Case 1: $\beta_{kj} \geq 1$*, No boundary intersection and* $R_\beta\left(\delta_{0,j,\nu}^\star, h_{km}\right) > R_\beta\left(\delta_{T,j,\nu}^\star, h_{km}\right) + vT$*:* In this case, $\mathcal{B}\left(x_0, R_\beta\left(\delta_{0,j,\nu}^\star, h_{km}\right)\right) \supset \mathcal{B}\left(x_T, R_\beta\left(\delta_{T,j,\nu}^\star, h_{km}\right)\right)$ and $\cup_{t\in[0,T]}\mathcal{B}\left(x_t, r_t\right) = \mathcal{B}\left(x_0, R_\beta\left(\delta_{0,j,\nu}^\star, h_{km}\right)\right)$. Thus, $\mathcal{A}_1\left(v, T, \delta_{0,j,\nu}^\star, \theta_0, \beta_{kj}, h_{j\nu}, h_{km}\right) = \mathcal{B}\left(x_0, R_\beta\left(\delta_{0,j,\nu}^\star, h_{km}\right)\right) \setminus \mathcal{B}\left(x_0, R_\beta\left(\delta_{0,j,\nu}^\star, h_{km}\right)\right) = 0$.

Case 2: $\beta_{kj} \geq 1$*, No boundary intersection and* $R_\beta\left(\delta_{T,j,\nu}^\star, h_{km}\right) > R_\beta\left(\delta_{0,j,\nu}^\star, h_{km}\right) + vT$*:* In this case, $\mathcal{B}\left(x_0, R_\beta\left(\delta_{0,j,\nu}^\star, h_{km}\right)\right) \subset \mathcal{B}\left(x_T, R_\beta\left(\delta_{T,j,\nu}^\star, h_{km}\right)\right)$ and thus, $\mathcal{A}_2\left(v, T, \delta_{0,j,\nu}^\star, \theta_0, \beta_{kj}, h_{j\nu}, h_{km}\right) = \mathcal{B}\left(x_T, R_\beta\left(\delta_{T,j,\nu}^\star, h_{km}\right)\right) \setminus \mathcal{B}\left(x_0, R_\beta\left(\delta_{0,j,\nu}^\star, h_{km}\right)\right)$.

Case 3: $\beta_{kj} \geq 1$ *and Boundaries intersects:* In this case, $\left|R_\beta\left(\delta_{T,j,\nu}^\star, h_{km}\right) - R_\beta\left(\delta_{0,j,\nu}^\star, h_{km}\right)\right| < vT$ and $\left|R_\beta\left(\delta_{T,j,\nu}^\star, h_{km}\right) + R_\beta\left(\delta_{0,j,\nu}^\star, h_{km}\right)\right| > vT$. $\mathcal{B}\left(x_0, R\left(\delta_{0,j,\nu}^\star, h_{km}\right)\right)$ and $\mathcal{B}\left(x_T, R\left(\delta_{T,j,\nu}^\star, h_{km}\right)\right)$ intersect. The void region is the crescent given as $\mathfrak{C} = \mathcal{B}\left(x_T, R_\beta\left(\delta_{T,j,\nu}^\star, h_{km}\right)\right) \setminus \mathcal{B}\left(x_0, R_\beta\left(\delta_{0,j,\nu}^\star, h_{km}\right)\right)$. Area of $\mathfrak{C}$ is calculated using formula for area of the lune, and is given in (13), where $r_0 = \sqrt{{\delta_{0,j,\nu}^\star}^2 - h_{j\nu}^2}$ [14].

Case 4: $\beta_{kj} \geq 1$*, No Intersection and Not Subset:* In this case, $\mathcal{B}\left(x_0, R_\beta\left(\delta_{0,j,\nu}^\star, h_{km}\right)\right)$ and $\mathcal{B}\left(x_T, R_\beta\left(\delta_{T,j,\nu}^\star, h_{km}\right)\right)$ are disjoint and not a subset of each other and thus, $\mathcal{A}_4\left(v, T, \delta_{0,j,\nu}^\star, \theta_0, \beta_{kj}, h_{j\nu}, h_{km}\right) = \left(\mathcal{B}\left(x_0, R_\beta\left(\delta_{0,j,\nu}^\star, h_{km}\right)\right) \cup \mathcal{B}\left(x_T, R_\beta\left(\delta_{T,j,\nu}^\star, h_{km}\right)\right)\right) \setminus \mathcal{B}\left(x_0, R_\beta\left(\delta_{0,j,\nu}^\star, h_{km}\right)\right) = \mathcal{B}\left(x_T, R_\beta\left(\delta_{T,j,\nu}^\star, h_{km}\right)\right)$.

Case 5: $\beta_{kj} < 1$*:* When $\beta_{kj} < 1$, the radius of circular void region shrinks and in this case, for each position of the UE, we get a circular void region with radius, $R_\beta\left(\delta_{t,j,\nu}^\star, h_{km}\right) = \sqrt{\beta_{kj}^2 {\delta_{t,j,\nu}^\star}^2 - h_{km}^2} = \sqrt{R_\beta\left(\delta_{0,j,\nu}^\star, h_{km}\right)^2 + \beta_{kj}^2 v^2 t^2 - 2\beta_{kj}^2 r_0 vt\cos\left(\theta_0\right)}$. Different from [13] where an approximation was adopted for calculating the area for this case, we find exact area expression using the theory of envelop of family of curves [15]. In this case, $\mathcal{A}_5\left(v, T, \delta_{0,j,\nu}^\star, \theta_0, \beta_{kj}, h_{j\nu}, h_{km}\right) = \cup_{t\in[0,T]}\mathcal{B}\left((vt, 0), R_\beta\left(\delta_{t,j,\nu}^\star, h_{km}\right)\right) \setminus \mathcal{B}\left(x_0, R_\beta\left(\delta_{0,j,\nu}^\star, h_{km}\right)\right)$ is a region which is a union of family of circles with varying centers and radius. The center is determined by UE position and the radius is given as $R_\beta\left(\delta_{t,j,\nu}^\star, h_{km}\right)$. Integrating the envelop of this family of circles will yield the required void area. The equation of *envelop* of this family of circles is

$$y = \sqrt{\frac{\left(x - \beta_{kj}^2 r_0\cos\left(\theta_0\right)\right)^2}{\left(1-\beta_{kj}^2\right)} - x^2 + R_\beta^2\left(\delta_{0,j,\nu}^\star, h_{km}\right)}. \tag{14}$$

Above equation is valid for a region $a < x < b$, where a and b are the x-coordinate of intersection points of the adjacent circular void regions about 0 and vT, respectively. Using circular geometry, We obtain these intersection points as $a = \beta_{kj}^2 r_0\cos\left(\theta_0\right)$ and $b = \beta_{kj}^2 r_0\cos\left(\theta_0\right) + vT\left(1-\beta_{kj}^2\right)$, respectively. Before a, the void region is the ball $\mathcal{B}\left(x_0, R_\beta\left(\delta_{0,j,\nu}^\star, h_{km}\right)\right)$ and beyond b, the void region is the ball $\mathcal{B}\left(x_T, R_\beta\left(\delta_{T,j,\nu}^\star, h_{km}\right)\right)$. Using (14), $\mathcal{A}_5\left(v, T, \delta_{0,j,\nu}^\star, \theta_0, \beta_{kj}, h_{j\nu}, h_{km}\right)$ is given in (15). A factor of 2 is multiplied due to symmetry of the void region.

Proposition 5. *The void area expression for a K-tier aerial network where each tier has DBSs at M possible altitudes and a variable CRE bias factor, B_k, is given in* (16)*.*

Proof: The details are given in the aforementioned Cases 1-5. The limits for each case are obtained after some mathematical manipulation. Due to space limitation, Case 5 is discussed briefly and the detailed proof is omitted. ∎

Proposition 6. *The probability of handover of a UE moving with velocity v for a time duration of T in a K-tier aerial network where each tier has DBSs at M possible altitudes and a variable CRE bias factor, B_k, is given in* (19)*, where θ_0 is a uniform random variable in the range $[0, \pi]$, $f_{\delta_{0,j,\nu}^\star}\left(\cdot|\mathbb{A}_{j,\nu}^\star\right)$ is given in* (9) *and $\Pr\left(\mathbb{A}_{j,\nu}^\star\right)$ is given in* (6)*.*

Proof:

Given that at time $t = 0$, the UE is connected to a tier-j DBS at height $h_{j\nu}$ and moves from x_0 to $x_T = (vT, 0)$, the conditional probability that handoff will not occur is given as

$$\Pr\left(\mathbb{N}_\mathbb{H}|\mathbb{A}_{j,\nu}^\star, \delta_{0,j,\nu}^\star, \theta_0\right) = \prod_{\{k,m\}} \Pr\left(\Phi_{km}\left(\mathcal{A}\left(v, T, \delta_{0,j,\nu}^\star, \theta_0, \beta_{kj}, h_{j\nu}, h_{km}\right)\right) = 0|\mathbb{A}_{j,\nu}^\star, \delta_{0,j,\nu}^\star, \theta_0\right). \tag{17}$$

The unconditional probability of no handover is obtained by averaging (17) over the distribution of $\delta_{0,j,\nu}^\star$, θ_0 and $\mathbb{A}_{j,\nu}^\star$ as

$$\Pr\left(\mathbb{N}_\mathbb{H}\right) = \sum_j \sum_\nu \Pr\left(\mathbb{A}_{j,\nu}^\star\right) \int_\delta \int_\theta \Pr\left(\mathbb{N}_\mathbb{H}|\mathbb{A}_{j,\nu}^\star, \delta, \theta\right) f_{\delta_{0,j,\nu}^\star}\left(\delta|\mathbb{A}_{j,\nu}^\star\right) f_{\theta_0}(\theta) d\delta d\theta. \tag{18}$$

For a PPP, $\Pr\left(\mathbb{N}_\mathbb{H}|\mathbb{A}_{j,\nu}^\star, \delta, \theta\right) = \exp\left(-\sum_{\{k,m\}} \lambda_{km}\left|\mathcal{A}\left(v, T, \delta_{0,j,\nu}^\star, \theta_0, \beta_{kj}, h_{j\nu}, h_{km}\right)\right|\right)$.

$$\left|\mathcal{A}_3\left(v,T,\delta^{\star}_{0,j,\nu},\theta_0,\beta_{kj},h_{j\nu},h_{km}\right)\right| = \left(R^2_{\beta}\left(\delta^{\star}_{0,j,\nu},h_{km}\right)+\beta^2_{kj}v^2T^2-2\beta^2_{kj}r_0vT\cos\left(\theta_0\right)\right)asec\left(\frac{2\sqrt{R^2_{\beta}\left(\delta^{\star}_{0,j,\nu},h_{km}\right)+\beta^2_{kj}v^2T^2-2\beta^2_{kj}r_0vT\cos\left(\theta_0\right)}}{2\beta^2_{kj}r_0\cos\left(\theta_0\right)-\left(\beta^2_{kj}+1\right)vT}\right)$$
$$-R^2_{\beta}\left(\delta^{\star}_{0,j,\nu},h_{km}\right)asec\left(\frac{2R_{\beta}\left(\delta^{\star}_{0,j,\nu},h_{km}\right)}{2\beta^2_{kj}r_0\cos\left(\theta_0\right)-\left(\beta^2_{kj}-1\right)vT}\right)+\frac{1}{2}vT\sqrt{4R^2_{\beta}\left(\delta^{\star}_{0,j,\nu},h_{km}\right)-\left(\left(1-\beta^2_{kj}\right)vT+2\beta^2_{kj}r_0\cos\left(\theta_0\right)\right)^2} \tag{13}$$

$$\left|\mathcal{A}_5\left(v,T,\delta^{\star}_{0,j,\nu},\theta_0,\beta_{kj},h_{j\nu},h_{km}\right)\right| = -\pi R^2_{\beta}\left(\delta^{\star}_{0,j,\nu},h_{km}\right)+2\int_{-R_{\beta}\left(\delta^{\star}_{0,j,\nu},h_{km}\right)}^{a}\sqrt{R^2_{\beta}\left(\delta^{\star}_{0,j,\nu},h_{km}\right)-x^2}dx$$
$$+2\int_a^b\sqrt{\frac{1}{\left(1-\beta^2_{kj}\right)}\left(x-\beta^2_{kj}r_0\cos\left(\theta_0\right)\right)^2-x^2+R^2_{\beta}\left(\delta^{\star}_{0,j,\nu},h_{km}\right)}dx+2\int_b^{vT+R_{\beta}\left(\delta^{\star}_{T,j,\nu},h_{km}\right)}\sqrt{R^2_{\beta}\left(\delta^{\star}_{T,j,\nu},h_{km}\right)-(x-vT)^2}dx \tag{15}$$

$$\left|\mathcal{A}\left(v,T,\delta^{\star}_{0,j,\nu},\theta_0,\beta_{kj},h_{j\nu},h_{km}\right)\right| = \begin{cases}\left|\mathcal{A}_3\left(v,T,\delta^{\star}_{0,j,\nu},\theta_0,\beta_{kj},h_{j\nu},h_{km}\right)\right| & \beta^2_{kj}\geq 1,\left(\beta^2_{kj}-1\right)vT-2R_{\beta}\left(\delta^{\star}_{0,j,\nu},h_{km}\right)<2\beta^2_{kj}r_0\cos\left(\theta_0\right)<\left(\beta^2_{kj}-1\right)vT+2R_{\beta}\left(\delta^{\star}_{0,j,\nu},h_{km}\right)\\ \pi\beta^2_{kj}\left(v^2T^2-2r_0vT\cos\left(\theta_0\right)\right) & \beta^2_{kj}\geq 1,2\beta^2_{kj}r_0\cos\left(\theta_0\right)<\left(\beta^2_{kj}-1\right)vT-2R_{\beta}\left(\delta^{\star}_{0,j,\nu},h_{km}\right)\\ 0 & \beta^2_{kj}\geq 1,2\beta^2_{kj}r_0\cos\left(\theta_0\right)>\left(\beta^2_{kj}-1\right)vT+2R_{\beta}\left(\delta^{\star}_{0,j,\nu},h_{km}\right),R_{\beta}\left(\delta^{\star}_{0,j,\nu},h_{km}\right)>vT,\\ \pi\left(R^2_{\beta}\left(\delta^{\star}_{0,j,\nu},h_{km}\right)+\beta^2_{kj}v^2T^2-2\beta^2_{kj}r_0vT\cos\left(\theta_0\right)\right) & \beta^2_{kj}\geq 1,2\beta^2_{kj}r_0\cos\left(\theta_0\right)>\left(\beta^2_{kj}-1\right)vT+2R_{\beta}\left(\delta^{\star}_{0,j,\nu},h_{km}\right),R_{\beta}\left(\delta^{\star}_{0,j,\nu},h_{km}\right)<vT,\\ \left|\mathcal{A}_5\left(v,T,\delta^{\star}_{0,j,\nu},\theta_0,\beta_{kj},h_{j\nu},h_{km}\right)\right| & \beta^2_{kj}<1,\end{cases} \tag{16}$$

Substituting $\Pr\left(\mathbb{N}_{\mathbb{H}}|\mathbb{A}^{\star}_{j,\nu},\delta,\theta\right)$ into (18), and using the fact that $\Pr\left(\mathbb{H}\right)=1-\Pr\left(\mathbb{N}_{\mathbb{H}}\right)$ yields (19). ∎

V. Numerical Results and Discussion

Numerical simulations were carried out in Python to analyze the performance of the K-tier aerial network with M-heights and to corroborate the derived analytical expressions. We simulated a 2-tier and a 3-tier network with M heights over an area of 1 square kilometer (km^2). The following parameters were set in the simulations unless stated otherwise: $P_k = 30$dBm, $\alpha = 3$, $T = 10s$, $\Lambda_1 = \Lambda_2 = 60$ DBSs per km^2, $K = 2$, $M = 1$. The number of Monte-Carlo simulation runs for each set of parameter values was 25000.

The probability of handover with varying velocity for a two-tier network is shown in Fig. 2. An obvious trend observed is that the handover probability increases with velocity. In Fig. 2(L), tier-1 and tier-2 DBSs are assumed be at the same altitude i.e., $h_{11} = h_{21} = 100m$ and the CRE factor is varied. It can be noted that the probability of handover is higher when $B_1 = B_2 = 1$. However, when the network is biased towards any one tier, i.e. $(B_1, B_2) = (3, 1)$ or $(B_1, B_2) = (1, 3)$, the probability of handover reduces. On the contrary, in Fig. 2(R), tier-1 and tier-2 have the same CRE factor i.e. $B_1 = B_2 = 1$ and the altitude of tiers is varied in the simulation i.e., $(h_{11}, h_{21}) = (100m, 100m)$, $(h_{11}, h_{21}) = (100m, 140m)$ or $(h_{11}, h_{21}) = (140m, 100m)$. Again in this case, the probability of handover is higher when $(h_{11}, h_{21}) = (100m, 100m)$. When altitude of any tier is increased, the probability of handover is reduced.

The reason for these trends is that decreasing CRE factor or increasing height of a tier, lowers the probability of association with that tier. As a result, the cell boundaries are dominated by the other tier which has the higher association probability due to higher CRE factor or lower height. This reduces the *effective density* of DBSs compared to the equal CRE and equal height scenario, in which the *effective* DBS density is the sum of both tiers i.e., $\Lambda_1 + \Lambda_2$. This lower *effective density* of the DBSs, dominates the cell boundaries, resulting in an increase in Voronoi cell size and hence a lower handover probability.

TABLE I: Simulation Parameters for Fig. 2 (3-Tier with 4 heights).

Algorithm	(h_{k1}, λ_{k1})	(h_{k2}, λ_{k2})	(h_{k3}, λ_{k3})	(h_{k4}, λ_{k4})
Tier-1	$(100, 40)$	$(100, 30)$	$(100, 20)$	$(100, 40)$
Tier-2	$(80, 20)$	$(90, 20)$	$(95, 20)$	$(100, 30)$
Tier-3	$(85, 20)$	$(100, 30)$	$(105, 20)$	$(100, 30)$

Furthermore, from Fig. 2 it can be observed that when a UE is connected to the tier with lower CRE factor, the probability of handover is higher because it is encouraged to offload to the other tier with the higher CRE factor. Similarly, the UE is encouraged to join the tier at a lower height and therefore, the probability of handover is higher when the UE is associated with the tier at higher altitude.

The handover probability for a 3-tier aerial network with $M = 4$ is plotted in Fig. 2(R). The height and corresponding densities of the DBSs are given in Table I. Again in this case the probability of handover increases with velocity. Moreover, the probability of handover is higher because a higher overall density leads to smaller cell sizes. The simulation results also corroborate the analytical results as shown in Fig. 2.

In Fig. 3, the probability of handover and probability of coverage (in terms of received signal strength (RSS)) for a two-tier network is plotted with varying the CRE factor. A low value of $\frac{B_2}{B_1}$ indicates that the UEs are forced to connect with tier-1 whereas a high value indicates that UEs are forced to connect with tier-2. It can be observed that, a high value of CRE factor reduces the probability of handover. The reasoning for this, as discussed above, is that the effective

$$\Pr(\mathbb{H}) = 1 - \sum_{j}\sum_{\nu} \Pr\left(\mathbb{A}^{\star}_{j,\nu}\right) \int_{\delta}\int_{\theta} \exp\left(- \sum_{\{k,m\}} \lambda_{km} \left| \mathcal{A}\left(v, T, \delta, \theta, \beta_{kj}, h_{j\nu}, h_{km}\right)\right| \right) f_{\delta^{\star}_{0,j,\nu}}\left(\delta | \mathbb{A}^{\star}_{j,\nu}\right) f_{\theta_0}(\theta) d\delta d\theta \quad (19)$$

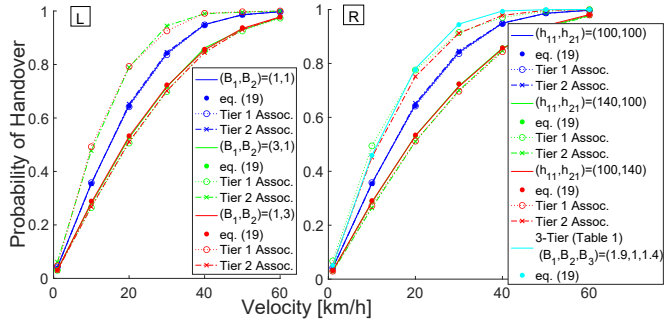

Fig. 2: Probability of handover with varying velocity.

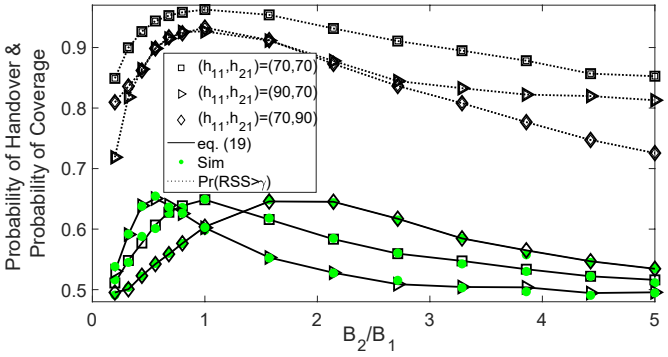

Fig. 3: Probability of handover and coverage for a two-tier network with varying the CRE and tier heights, where $T = 5s$ and $\gamma = 8$dB.

cell size increases because overall effective density of the DBSs is reduced. Alternatively, it can be reasoned that, when $\frac{B_2}{B_1}$ is high, handover only occurs within tier-2 (intra-tier handover). Similarly, when $\frac{B_2}{B_1}$ is low, handover occurs only within tier-1 DBSs and thus, the handover probability is lower. For intermediate values of $\frac{B_2}{B_1}$, DBSs of both tiers are active and inter-tier handover also occurs and the Voronoi cell size reduces and UE experience more number of handovers. Similar to Fig. 2, it can be noted that increasing the DBS altitude, reduces the handover probability. Again, in this case, the analytical results match the simulation results quite well.

It is desirable to lower the handover probability, as it reduces signaling overhead and load on the network. Above results indicate that either biasing towards another tier or increasing the height of a tier can reduce the probability of handover. However, this does not portray the complete picture. Reducing the DBS density impacts the RSS and reduces the probability of coverage. This tradeoff is shown clearly in Fig. 3. Therefore, when optimizing network parameters, handover probability must be optimized along with other affected parameters such as coverage probability and the network must be configured at a sweet spot where there is good coverage probability and a lower handover probability.

VI. CONCLUSION

In this work, the probability of handover of a K-tier aerial network is analyzed. The DBSs in each tier can hover at different altitudes and each tier has a different CRE factor. Simulation results, corroborating the analytical analysis, show that increasing altitude or the CRE factor reduces the handover probability. However, this comes at a cost of reduced coverage probability. Thus, when setting parameters to reduce handover probability, other KPIs such as coverage and RSRP must also be taken into account and be optimized jointly.

REFERENCES

[1] G. Geraci, A. Garcia-Rodriguez, M. M. Azari, A. Lozano, M. Mezzavilla, S. Chatzinotas, Y. Chen, S. Rangan, and M. D. Renzo, "What will the future of UAV cellular communications be? a flight from 5G to 6G," *IEEE Communications Surveys and Tutorials*, vol. 24, no. 3, pp. 1304–1335, Third Quater 2022.

[2] H. N. Qureshi and A. Imran, "On the tradeoffs between coverage radius, altitude, and beamwidth for practical UAV deployments," *IEEE Transactions on Aerospace and Electronic Systems*, vol. 55, no. 6, pp. 2805–2821, Jan. 2019.

[3] A. Imran, A. Zoha, and A. Abu-Dayya, "Challenges in 5G: how to empower SON with big data for enabling 5G," *IEEE Network*, vol. 28, no. 6, pp. 27–33, Nov. 2014.

[4] S. Sekander, H. Tabassum, and E. Hossain, "Multi-tier drone architecture for 5G/B5G cellular networks: Challenges, trends, and prospects," *IEEE Communications Magazine*, vol. 56, no. 3, pp. 96–103, Mar. 2018.

[5] S. M. A. Zaidi, M. Manalastas, H. Farooq, and A. Imran, "Mobility management in emerging ultra-dense cellular networks: A survey, outlook, and future research directions," *IEEE Access*, vol. 8, pp. 183 505–183 533, Sep. 2020.

[6] H. Tabassum, M. Salehi, and E. Hossain, "Fundamentals of mobility-aware performance characterization of cellular networks: A tutorial," *IEEE Communications Surveys & Tutorials*, vol. 21, no. 3, pp. 2288–2308, Third Quarter. 2019.

[7] S.-Y. Hsueh and K.-H. Liu, "An equivalent analysis for handoff probability in heterogeneous cellular networks," *IEEE Communications Letters*, vol. 21, no. 6, pp. 1405–1408, Jun. 2017.

[8] W. Huang, H. Zhang, and M. Zhou, "Analysis of handover probability based on equivalent model for 3D UAV networks," in *2019 IEEE 30th Annual International Symposium on Personal, Indoor and Mobile Radio Communications (PIMRC), Istanbul, Turkey*, 2019, pp. 1–6.

[9] M. Banagar, V. V. Chetlur, and H. S. Dhillon, "Handover probability in drone cellular networks," *IEEE Wireless Communications Letters*, vol. 9, no. 7, pp. 933–937, Jul. 2020.

[10] M. Salehi and E. Hossain, "Handover rate and sojourn time analysis in mobile drone-assisted cellular networks," *IEEE Wireless Communications Letters*, vol. 10, no. 2, pp. 392–395, Feb. 2021.

[11] R. Amer, W. Saad, and N. Marchetti, "Mobility in the sky: Performance and mobility analysis for cellular-connected UAVs," *IEEE Transactions on Communications*, vol. 68, no. 5, pp. 3229–3246, May 2020.

[12] R. Arshad, H. Elsawy, L. Lampe, and M. J. Hossain, "Handover rate characterization in 3D ultra-dense heterogeneous networks," *IEEE Transactions on Vehicular Technology*, vol. 68, no. 10, pp. 10 340–10 345, Oct. 2019.

[13] M. Salehi and E. Hossain, "Stochastic geometry analysis of sojourn time in multi-tier cellular networks," *IEEE Transactions on Wireless Communications*, vol. 20, no. 3, pp. 1816–1830, Mar. 2021.

[14] E. W. Weisstein, *Lune*. From MathWorld–A Wolfram Web Resource., https://mathworld.wolfram.com/Lune.html.

[15] J. W. Bruce and P. J. Giblin, *Curves and Singularities: A Geometrical Introduction to Singularity Theory*, 2nd ed. Cambridge University Press, 1992.